H1prelim-12-131
March 2014

Submitted to

Rencontres de Moriond, QCD and High Energy Interactions, March 22-23, 2014, La Thuile,Valle d'Aosta, Italy
Abstract: **xx-xxx**
Parallel Session **x**

Electronic Access: www-h1.desy.de/h1/www/publications/conf/conf_list.html

Search for QCD Instanton-Induced Processes in Deep-Inelastic Scattering at HERA (version of March 14, 2014)

H1 Collaboration

Abstract

Signals of QCD instanton-induced processes are searched for in deep-inelastic scattering (DIS) at the electron-proton collider HERA in the kinematic region defined by the Bjorken-scaling variable $x > 10^{-3}$, the inelasticity $0.2 < y < 0.7$ and the photon virtuality $150 < Q^2 < 15000$ GeV^2. The search is performed using H1 data corresponding to an integrated luminosity of 357 pb^{-1}. Several observables of the hadronic final state of the events are exploited to identify a potentially instanton-enriched domain. Two Monte Carlo models, RAPGAP and DJANGOH, are used to estimate the background from the standard DIS processes, and the instanton-induced scattering processes are modeled by the program QCDINS. In order to extract the expected signal a multivariate data analysis technique is used.

1 Introduction

The Standard Model of particle physics contains anomalous processes which violate the conservation of baryon and lepton number $(B + L)$ in the case of electroweak interactions and chirality in the case of strong interactions [1]. Such anomalous processes are induced by instantons [1, 2]. In quantum chromodynamics (QCD), theory of the strong interactions, instantons are non-perturbative fluctuations of the gluon field. and they can be interpreted as tunnelling transitions between topologically non-equivalent vacua. Deep-inelastic scattering (DIS) offers a unique opportunity [3] to discover a class of hard processes induced by QCD instantons. The cross-section is calculable within "instanton-perturbation theory" and is found to be sizeable [4–6]. Moreover, the instanton-induced final state exhibits a characteristic signature [3, 7–10]. Detailed reviews are given in Refs. [11, 12] and the short overview can be find in Ref. [13].

An experimental observation of instanton-induced processes would constitute a discovery of a basic and novel non-perturbative QCD effect at high energies. The theory and phenomenology for the production of instanton-induced processes at HERA in electron [1] proton collisions at a centre of mass energy of 300 GeV has been worked out by Ringwald and Schrempp [3–8]. The size of the predicted cross-section is large enough to make an experimental observation possible. The expected signal rate is, however, still small compared to that from the standard DIS process. The suppression of the standard DIS background is therefore the key issue in this analysis. QCD instanton-induced processes can be discriminated from standard DIS by their characteristic hadronic final state signature, consisting of a large number of hadrons at high transverse energy emerging from a "fire-ball"-like topology in the instanton rest system [3, 7, 8]. Derived from simulations studies characteristic observables are exploited to identify a phase space region where a difference between data and the standard DIS simulations would indicate a contribution from instanton-induced processes.

Upper cross-section limits on instanton-induced processes have been reported by H1 [13] and ZEUS [14] collaborations. This analysis is the continuation of H1 searches for instanton-induced events in the kinematical domain recommended by instanton perturbation theory using about seventeen times larger data sample .

2 Phenomenology of QCD Instanton-Induced Processes in DIS

According to Ringwald and Schrempp [3–8], instanton (I) processes dominantly occur in a photon gluon (γg) fusion process as sketched in Fig. 1. The characteristic I-event signatures result from the following basic reaction:

$$\gamma^* + g \overset{(I)}{\rightarrow} \sum_{n_f} (q_R + \bar{q}_R) + n_g\, g, \quad (I \rightarrow \bar{I}, R \rightarrow L), \tag{1}$$

[1] The term "electron" is used in the following to refer to both electron and positron.

where g, q_R ($\bar{q}_R$) denotes gluons, right-handed quarks (anti-quarks), n_f is the number of quark flavours and n_g is the number of gluons produced. Right-handed quarks are produced in I-induced processes, left-handed quarks are produced in anti-instanton ($\bar{I}$) processes. The final state induced by instantons or anti-instantons can only be distinguished by the chirality of the quarks. Experimental signatures sensitive to instanton-induced chirality violation are not exploited in this analysis. Both I-processes and $\bar{I}$-processes enter in the calculation of the total cross-section.

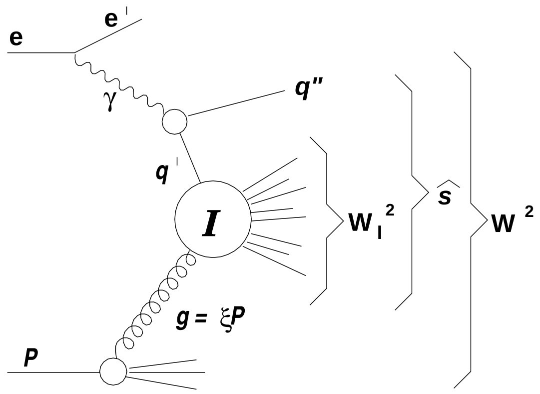

DIS variables:
$s = (e + P)^2$
$Q^2 = -\gamma^2 = -(e - e')^2$
$x = Q^2 / \; (2P \cdot \gamma)$
$y = Q^2 / \; (s \; x)$
$W^2 = (\gamma + P)^2 = Q^2(1 - x)/x$
$\hat{s} = (\gamma + g)^2$
$\xi = x \; (1 + \hat{s}/Q^2)$

Variables of I-subprocess:
$Q'^2 \; \equiv -q'^2 = -(\gamma - q'')^2$
$x' \equiv Q'^2 \; / \; (2 \; g \cdot q')$
$W_I^2 \equiv (q' + g)^2 = Q'^2 \; (1 - x' \;)/x'$

Figure 1: Kinematic variables of the dominant I-induced process in DIS. The virtual photon (4-momentum $\gamma = e - e'$), emitted by the incoming electron e, fuses with a gluon (4-momentum g) radiated from the proton (4-momentum P). The gluon carries a fraction ξ of the longitudinal proton momentum. The virtual quark entering the instanton subprocess has 4-momentum q', while the outgoing quark (= *current quark*) from the photon splitting process has q''. W_I is the invariant mass of the quark gluon ($q'g$) system and W is the invariant mass of the total hadronic system (the γP system). $\hat{s}$ is the invariant mass squared of the γg system.

As shown in Fig. 1, a photon splits into a quark anti-quark pair in the background of an instanton or an anti-instanton field. The so-called I-subprocess $q' + g \stackrel{(I,\bar{I})}{\rightarrow} X$ is produced by the quark or the anti-quark fusing with a gluon g from the proton. The respective partonic final state includes $2\,n_f - 1$ light quarks and anti-quarks. Therefore, together with the current quark (q''), in every I-event, quark anti-quark pairs of each of the $n_f (= 3)$ (light) flavours are simultaneously produced[2]. In addition, a mean number of $\langle n_g \rangle \sim \mathcal{O}(1/\alpha_s) \sim 3$ gluons is expected to be emitted in the I-subprocess.

The quarks and gluons emerging from the I-subprocess are isotropically distributed in the I-rest system defined by $\vec{q'} + \vec{g} = 0$. One expects therefore a pseudo-rapidity[3] (η) region with a

[2] In principle, also heavy flavours contribute whenever very small instantons are probed. In general, however, the quarks must appear approximately massless on the scale of the dominant effective I-size $\rho_{\rm eff}(Q'^2, x')$, i.e. $\rho_{\rm eff}\, m_q \ll 1$, where m_q is the quark mass. In the HERA kinematic region, the rate is dominated by $\rho_{\rm eff} \approx 0.35$ fm such that only up, down and strange quarks appear massless ($n_f = 3$). The contribution of charm and bottom quarks to the cross-section is likely to be small. It was checked that the predicted final state signature does not change significantly if heavy quarks are included in the simulation.

[3] The pseudo-rapidity of a particle is defined as $\eta \equiv -\ln\tan(\theta/2)$, where θ is the polar angle with respect to the proton direction defining the $+z$-axis.

width of typically 2 units in η. This region is densely populated with particles of relatively high transverse momentum which are homogeneously distributed in azimuth in the I-rest frame. Apart from this pseudo-rapidity band, the hadronic final state exhibits a current jet emerging from the outgoing current quark q''. The large number of partons emitted in the I-process leads to a high multiplicity of charged and neutral particles in every event.

The actual number of produced hadrons and their energies crucially depends on the centre of mass energy W_I available in the I-system, which in turn can be written (see Fig. 1) in terms of the variables Q'^2 and x' describing the kinematics of the I-subprocess. These variables are defined in analogy to the Bjorken scaling variables x and Q^2. A knowledge of the distributions of these variables is indispensable for the correct prediction of the hadronic final state. These distributions can be calculated within I-perturbation theory [4, 5] for large Q'^2 and x'.

The total I-production cross-section at HERA, $\sigma^{(I)}_{\rm HERA}$, is essentially determined by the cross-section of the I-subprocess $q' + g \xrightarrow{(I)} X$ denoted by $\sigma^{(I)}_{q'g}$ and is calculable in I-perturbation theory. The qualitative behaviour for the I-cross-section:

$$\sigma^{(I)}_{q'g} \sim \left[\frac{2\pi}{\alpha}\right]^{12} e^{-\frac{4\pi}{\alpha}} \tag{2}$$

shows strong dependence of the cross section on strong coupling α_s.

In the kinematic domain in which this analysis is performed, i.e. $0.2 < y < 0.7$, $x > 10^{-3}$ and $150 < Q^2 < 15000\ \mathrm{GeV}^2$, the cross-section calculated with QCDINS is $\sigma^{(I)}_{\rm HERA} = 10^{+2}_{-2}$ pb using the 2010 world average of the strong coupling, $\alpha_s(M_Z) = 0.1184 \pm 0.0007$, $\Lambda^{(5)}_{\overline{MS}} = 213^{+9}_{-9}\ \mathrm{MeV}$ [20]. The quoted errors for the I-induced cross-section $\sigma^{(I)}_{\rm HERA}$ only contain the uncertainty obtained from varying the strong coupling.

Even though these predictions have not yet reached the same quantitative level of precision as current standard perturbative QCD calculations, the cross-section is large enough to motivate dedicated searches for I-processes at HERA.

3 Experimental Method

3.1 The H1 Detector

A detailed description of the H1 detector can be found elsewhere [21–24]. Only the components essential to the present analysis are described here. The origin of the H1 coordinate system is the nominal ep interaction point. The direction of the proton beam defines the positive z–axis (forward direction). The polar angles θ and transverse momenta P_T of all particles are defined with respect to this axis. The azimuthal angle ϕ defines the particle direction in the transverse plane. The pseudorapidity is defined as $\eta = -\ln\tan\frac{\theta}{2}$. The detector components most relevant to this analysis are the Liquid Argon (LAr) calorimeter, which measures the positions and energies of particles over the range $4^\circ < \theta < 154^\circ$ with full azimuthal coverage, the inner tracking detectors, which measure the angles and momenta of charged particles over the range $7^\circ < \theta < 165^\circ$, and a lead-fibre calorimeter (SpaCal) covering the range $153^\circ < \theta < 177^\circ$.

The LAr calorimeter consists of an electromagnetic section with lead absorbers and a hadronic section with steel absorbers. The electromagnetic and the hadronic sections are highly segmented in the transverse and the longitudinal directions. Electromagnetic shower energies are measured with a resolution of $\delta E/E \simeq 0.11/\sqrt{E/\mathrm{GeV}} \oplus 0.01$ and hadronic energies with $\delta E/E \simeq 0.46/\sqrt{E/\mathrm{GeV}} \oplus 0.03$ as determined using electron and pion test beam data [25,26].

In the central region, $25^\circ < \theta < 155^\circ$, the central tracking detector (CTD) measures the trajectories of charged particles in two cylindrical drift chambers immersed in a uniform $1.16\,\mathrm{T}$ solenoidal magnetic field. In addition, the CTD contains a drift chamber (COZ) to improve the z coordinate reconstruction and a multi-wire proportional chamber at inner radii (CIP) mainly used for triggering [27]. The CTD measures charged particles with a transverse momentum resolution of $\sigma(p_T)/p_T \simeq 0.2\%\, p_T/\mathrm{GeV} \oplus 1.5\%$. The forward tracking detector (FTD) is used to supplement track reconstruction in the region $7^\circ < \theta < 30^\circ$ [28] and improves the hadronic final state reconstruction of forward going low momentum particles.

The CTD tracks are linked to hits in the vertex detectors: the central silicon tracker (CST) [29, 30], the forward silicon tracker (FST) [31], and the backward silicon tracker (BST) [32]. These detectors provide precise spatial track reconstruction and therefore also improve the primary vertex spatial reconstruction.

In the backward region the SpaCal provides an energy measurement for hadronic particles, and has a hadronic energy resolution of $\delta E/E \simeq 0.70/\sqrt{E/\mathrm{GeV}} \oplus 0.01$ and a resolution for electromagnetic energy depositions of $\delta E/E \simeq 0.07/\sqrt{E/\mathrm{GeV}} \oplus 0.01$ measured using test beam data [33].

The ep luminosity is determined by measuring the event rate for the Bethe-Heitler process $ep \rightarrow ep\gamma$ where photon is detected in the photon tagger located at $z = -103\,\mathrm{m}$. The overall normalisation is determined using a precision measurement of the QED Compton process [34] and erratum to it.

3.2 The Trigger

NC events at high Q^2 are triggered mainly using information from the LAr calorimeter. The calorimeter has a finely segmented pointing geometry allowing the trigger to select localised energy deposits in the electromagnetic section of the calorimeter pointing to the nominal interaction vertex. For electrons with energy above $11\,\mathrm{GeV}$ the trigger efficiency is determined to be almost 100% [35].

3.3 Data Samples

This analysis is performed using the full $e^{\pm}p$ collision data set taken in the years 2004-2007 by the H1 experiment. The data were recorded with a lepton beam of energy 27.6 GeV and a proton beam of energy 920 GeV, corresponding to a centre-of-mass energy $\sqrt{s} = 319$ GeV. The total integrated luminosity of the analysed data is $357.6\,\mathrm{pb}^{-1}$.

4 Simulation of Standard DIS and I-Processes

Detailed simulation of the H1 detector response to hadronic final states have been performed for two QCD models of the standard DIS processes (background) and for QCD I-induced scattering processes (signal).

The RAPGAP Monte Carlo [36] incorporates the $\mathcal{O}(\alpha_s)$ QCD matrix element and models higher order parton emissions to all orders in α_s using the concept of parton showers [37] based on the leading logarithm DGLAP equations [38], where QCD radiation can occur before and after the hard subprocess.

An alternative treatment of the perturbative phase is implemented in DJANGOH [39]which uses Color Dipole Model [40] with QCD matrix element corrections as implemented in ARIADNE [41]. In both MC generators the hadronization is performed using the LUND string model [42] implemented in JETSET [43] and the CTEQ6L [44] parton density functions is used.

QCDINS [10,15] is a Monte Carlo package to simulate QCD I-induced scattering processes in DIS. It acts as a hard process generator embedded in the HERWIG [16] program. The hard process is treated according to the physics assumptions explained in section 2. The default parameters of the QCDINS 2.0 version were used, i.e. $x' > 0.35$, $Q'^2 > 113 \ \mathrm{GeV}^2$ and the number of flavours is set to $n_f = 3$. The CTEQ5L [45] parton density functions have been employed. After assembling the hard I-subprocess, further QCD emissions are simulated in the leading-logarithm approximation. The coherent branching algorithm implemented in HERWIG is used. The transition from partons to the observable hadrons is performed using JETSET.

5 Event Selection and Search Strategy

5.1 Inclusive DIS Event Selection

The NC DIS events which are primarily selected by requiring a scattered electron The scattered electron is identified as the compact cluster of energy deposit in the electromagnetic part of the LAr calorimeter with the highest transverse momentum. A minimal electron energy 11 GeV is required. The remaining clusters in the calorimeters and charged tracks are attributed to the hadronic final state (HFS) which is reconstructed using an energy flow algorithm without double counting of energy [46, 47]. The electromagnetic energy calibration and the alignment of the H1 detector are performed following the same procedure as in [48] and the HFS calibration is described in [35]. The longitudinal momentum balance is required to lie within 45 GeV $< \sum(E - p_z) < 65$ GeV, where the sum runs over the scattered electron and all HFS objects . Furthermore the position of the z coordinate of the reconstructed event vertex must be within ± 35 cm of the nominal interaction point.

The photon virtuality Q^2 and the Bjorken scaling variable x are reconstructed from the scattered electron and the hadronic final state particles using the electron-sigma methods [49]. The events are selected to cover the phase space region defined by $0.2 < y < 0.7$, $x > 10^{-3}$ and $150 < Q^2 < 15000 \ \mathrm{GeV}^2$.

The selection of events passing the above cuts provides the NC DIS sample which forms the basis of subsequent analysis. The selected DIS data sample consists of about 349000 events. The simulated events reproduce well the shape and the absolute normalisation of the distributions of the energy and angle of the scattered electron as well as the kinematic variables x, Q^2 and y.

5.2 Definition of the observables and Search Strategy

The observables used to discriminate the I-induced contribution from the standard DIS process are based on the hadronic final state. Only HFS objects with $\eta_{\rm Lab} < 3.2$ are considered. Charged particles with transverse momenta of $P_T > 0.12$ GeV are selected as central tracks within $\theta > 20^o$. Here, both $\eta_{\rm Lab}$ and P_T are measured in the laboratory frame.

All HFS objects are boosted to the hadronic centre-of-mass frame (HCM)[4]. Jets are defined by the inclusive k_T algorithm [50] as implemented in FastJet [51], with the massless P_T recombination scheme and with the distance parameter $R_0 = 1.35 \times R_{con}$ where a cone radius of $R_{con} = 0.5$ according with prescription in Ref. [50]. The jets are required to have the transverse energy $E_{T,Jet}> 3$ GeV. Additional requirements on the transverse energy and pseudorapidity of the jets in the laboratory frame, $-1.0 < \eta_{Jet}^{Lab} < 2.5$ and $E_{T,Jet}^{Lab} > 2.5$ GeV, are imposed in order to ensure that jets are contained within the acceptance of the LAr calorimeter and are well calibrated. The jet with the highest transverse energy $E_{T,Jet}> 4$ GeV is used to estimate the 4-momentum q'' of the current quark (see Fig. 1). Q'^2 can be reconstructed from the particles associated with the current jet and the photon 4-momentum, which is obtained using the measured momentum of the scattered electron. Due to the limited accuracy of the Q'^2 reconstruction, the reconstructed Q'^2 cannot be used to experimentally control the "true" Q'^2 region of the I-processes, but can nevertheless be exploited to discriminate I-processes from the standard DIS background. The reconstructed Q'^2 is called $Q'^2_{\rm rec}$ in what follows. More information on the Q'^2 reconstruction can be found in [8, 17, 18].

The hadronic final state objects belonging to the current jet are not used in the definition of the following observables. A band in pseudo-rapidity with a width of ± 1.1 units in η is defined around the centre of gravity $\bar{\eta} = \sum E_T \eta / (\sum E_T)$ of the transverse energy (E_T) distribution of the hadronic final state objects (see Ref. [18] for details). This pseudo-rapidity band is called the I-band in the following. The number of charged particles in the I-band measured as tracks in the detector is counted (n_B) and the total scalar transverse energy of all hadronic final state objects in the I-band is measured ($E_{T,B}$).

All hadronic final state objects in the I-band are boosted to an approximate I-rest frame defined by $\vec{q'} + \langle\xi\rangle \vec{P} = 0$, where $\langle\xi\rangle = 0.076$ is the average value expected by the QCDINS Monte Carlo simulation (see Fig. 1 for definition). In this system the sphericity ($\rm Sph_B$) and few Fox-Wolfram moments ($\rm H_{l0}$) are calculated[5]. For spherical events $\rm Sph_B$ is close to 1, while for pencil-like events $\rm Sph_B$ is 0. Furthermore, the axes $\vec{i}_{\rm min}$ and $\vec{i}_{\rm max}$ are found for which in the I-rest system the summed projections of the 3-momenta of all hadronic final state objects in the

[4]The hadronic centre-of-mass frame is defined by $\vec{\gamma} + \vec{P} = 0$, where $\vec{\gamma}$ ($\vec{P}$) is the 3-momentum of the exchanged photon (proton).

[5]The sphericity is defined as $\rm SPH = (3/2)(\lambda_2 + \lambda_3)$ where λ_2 and λ_3 are the smallest of the three eigenvalues

I-band are minimal or maximal [7]. The relative difference between $E_{IN} = \sum_h |\vec{p}_h \cdot \vec{i}_{\max}|$ and $E_{OUT} = \sum_h |\vec{p}_h \cdot \vec{i}_{\min}|$ is called $\Delta_B = (E_{IN} - E_{OUT})/E_{OUT}$. This quantity is a measure of the transverse energy weighted azimuthal isotropy of an event. For isotropic events Δ_B is small while for pencil-like events Δ_B is large.

The reconstruction of the variable x' is difficult. However using the boost to I-rest and all hadronic final state objects in the I-band x' is reconstructed as $x'_{rec} = (x'_1 + x'_2)/2$ where $x'_i = Q'^2_{\rm rec}/(W^2_{I,i} + Q'^2_{\rm rec})$ with $W^2_{I,1} = (q'_{rec} + \langle\xi\rangle P)^2$ and $W^2_{I,2} = (\sum_i v_{i,rec})^2_{Band}$. And as in case of $Q'^2_{\rm rec}$ the reconstructed x'_{rec} cannot be used to experimentally control the "true" x' region of the I-processes, but can be used to discriminate I-processes from the standard DIS background.

Five observables are used to enhance the fraction of I-events in the inclusive data sample: the charged particle multiplicity in the I-band (n_B), the transverse energy of reconstructed current jet $E_{T,Jet}$, two quantities measuring the azimuthal isotropy of an event E_{IN}, Δ_B and the reconstructed kinematical variable of I-subprocess x'_{rec}. Other observables are used for further checks: the reconstructed instanton kinematic variable, $Q'^2_{\rm rec}$, the total scalar transverse energy of all hadronic final state objects in the I-band,$E_{T,B}$, two variables measuring the azimuthal isotropy of the event E_{OUT} and Sph_B, and the Fox-Wolfram moment H_{10}.

5.3 Systematic uncertainties

The following sources of systematic uncertainties are taken into account:

- The uncertainty of the energy scale of the HFS 1%.
- The energy of the scattered electron is measured with precision $0.5 - 1\%$.
- The precision of the electron polar angle measurement is 1 mrad.
- Depending on electron polar angle the uncertainty on the electron identification is $0.5 - 2\%$.
- The uncertainty associated with the track reconstruction is estimated to be 0.5%.
- The effect of the nuclear interaction in the detector material on the efficiency of track reconstruction is 0.5%.

These uncertainties have been propagated into the overall systematic error. The effect of the above uncertainties on the expectation is determined by varying the correspondinq quantities by ± 1 standard deviation in the MC samples and propagating these variations through the whole analysis. The main contributions to the systematic uncertainties are seen to arise from the the energy of the scattered electron, from $\sim 4\%$ in the background dominated region to $\sim 1\%$

of the diagonalised sphericity tensor defined by $S^{\alpha\beta} = (\sum_i p_i^\alpha p_i^\beta)/\sum_i |p_i|^2$, where α and β corresponds to the x, y and z components of the considered particle momenta p_i [52].

The Fox-Wolfram moments are defined as $H_l = \sum_{i,j}^N \frac{|\vec{p}_i||\vec{p}_j|}{E^2_{\rm tot}} P_l(\cos\Theta_{ij})$, where Θ_{ij} is the opening angle between hadrons i and j and $E^2_{\rm tot}$ is the total energy, and the P_l are the Legendre polynomials. The normalised moments are define by $H_{l0} = H_l/H_0$ [52, 53].

in the signal region, and the energy scale of the HFS, from $\sim 1\%$ in the background region to $\sim 2.5\%$ in the signal region. The uncertainties connected with the nuclear interaction and the track reconstruction contribute to the systematic error mainly in the signal region, $\sim 2\%$ each, and less than 0.5% in background dominated region. The result of the uncertainty on the electron identification and the precision of the electron polar angle is small ($< 0.5\%$) in the full range of the discriminator.

The additional systematic uncertainties are included in the exclusion limit calculation:

- The normalisation uncertainty due to the precision of the luminosity measurement is 2.3%.
- The difference between DJANGOH and RAPGAP predictions is assigned as the model uncertainty of the background estimation.
- The uncertainty of the relative background normalisation[6] is 1.1%.
- The uncertainty of the predicted signal cross section is 20% (section 2).

5.4 Comparison of Data to Standard QCD Prediction

Both RAPGAP and DJANGOH simulations provide a good overall description of the experimental data in the inclusive and the jet sample. To further improve the agreement between Monte Carlo simulation and data, the jet multiplicities are reweighted as a function of Q^2 and additionally, the MC events are reweighted as function of P_T and η of the most forward jet in the Breit frame [35, 54]. Additionally, the track multiplicity distribution is reweighting. The weights are obtained from the ratio of data to the reconstructed MC distributions and are applied to events on generator level. After these reweightings, the simulations provide a good description of the shapes and normalisation of all data distributions.

The distributions of the five observables $E_{T,Jet}$, n_B, x'_{rec}, Δ_B and E_{IN} for data, for two standard DIS QCD models and for the I-process are shown in Fig. 2. The instanton prediction is shown as a smooth line and for visibility it is scaled up by a factor 50. The gross features of the data are reasonably well described by both Monte Carlo simulations. The models are able to describe the data within $5 - 10\%$ except at very low and/or very large values of the given observable where a difference up to 20% is observed.

In addition, the Fig. 3 shows the distribution of the other observables.

[6]This uncertainty is defined as:

$$\epsilon = (\int dD(\frac{dn}{dD})_{Dj} - \int dD(\frac{dn}{dD})_{Rap})/\int dD(\frac{dn}{dD})_{DJ} \qquad (3)$$

where $(\frac{dn}{dD})_{Dj}$ and $(\frac{dn}{dD})_{Rap}$ are the discriminator distributions (section 6) for the DJANGOH and RAPGAP MC,respectively.

6 Search for Instanton-Induced Events

The multivariate discrimination technique is employed to increase the sensitivity to I-processes. Four methods as implemented in TMVA ROOT package [55] was used: PDERS (*Probability Density Estimator with Range Search*), neural network MLP (*Multi-Layer Perceptron*) and two variants of decision tree BDT (*Boosted Decision Trees*), BDTG (*Boosted Decision Trees with Gradient Boost*). The results are presented for PDERS method, three other methods give similar results.

The strategy to reduce the standard DIS background is based on the observables: $E_{T,Jet}$, n_B, x'_{rec}, Δ_B and E_{IN}. These observables have been chosen, since they provide the best signal to background separation. Moreover, their distributions are well described by both Monte Carlo simulations and finally, taking into account the systematic uncertainties, the resulting discriminator distribution is satisfactory described by Monte Carlo simulation in the background dominated region.

Fig. 4 shows the absolutely normalised discriminator distribution in the logarithmic scale and Fig. 5 show same distribution in the linear scale. The simulated background events are mainly concentrated at low D values while the simulated I-signal events are peaked at the large D values. Towards larger D values the background falls by order of magnitudes. The data roughly follow this trend. In the expected instanton dominated region, no excess of event is observed. The DJANGOH Monte Carlo describes the data, while RAPGAP is above data.

The method to minimise the statistical error on the cross section for the hypothetical instanton signal is used to calculate the cut value D_{cut} defining the signal region. In case of PDERS method, this value is $D_{cut} = 0.86$. The region dominated by the expected instanton signal is presented in more detail in Fig. 6. In the signal region, the additional observables unused in the PDERS method are shown in Fig. 7 and the lack of any event excess is clearly visible.

	Multivariate method			
	PDERS	MLP	BDT	BDTG
Data	2492	2647	2395	2566
DJANGOH	2483^{+77}_{-91}	2718^{+84}_{-98}	2452^{+79}_{-83}	2630^{+79}_{-93}
RAPGAP	2966^{+91}_{-104}	3201^{+101}_{-102}	2906^{+93}_{-88}	3120^{+95}_{-99}
QCDINS	521^{+10}_{-13}	524^{+11}_{-13}	501^{+10}_{-13}	531^{+11}_{-13}

Table 1: Number of events observed in the data and expected from the DJANGOH and RAPGAP simulation after optimising the I-signal to background ratio. The quoted error contains the full statistical and systematic uncertainty added in quadrature.

In the signal region, 2492 events are observed in the data, while 2483^{+77}_{-91} (2966^{+91}_{-104}) are expected for DJANGOH (RAPGAP). In table 1 the results for the other methods are presented.

Since no evidence for QCD instanton-induced processes is observed, the data are used to set the exclusion limit.

7 Exclusion Limits for Instanton-induced Processes

The upper limit is determined from a CL_s statistical analysis [56, 57] using the the method of fractional event counting, optimised for the presence of systematic uncertainties [58]. A test statistic X is constructed as a fractional event count of all events using the discriminator histogram:

$$X = \sum_{i=1}^{N_{\mathrm{bin}}} w_i n_i \,, \tag{4}$$

where the sum runs over all bins and n_i is the number of events observed in bin i. The weights w_i, solutions of the appropriate set of linear equations, are defined in such a way as to unsure that only bins with both a large signal contribution and small systematic uncertainties enter with sizeable weights into the test statistic X. In case of negligible systematic uncertainties, the weights behave as $w_i = s_i/(s_i + 2b_i)$ where s_i and b_i are the predicted a signal and background number of events for a given i bin, respectively. A large number of MC experiments are generated by varying the expected number of events $s_i + b_i$ within the uncertainties. Systematic uncertainties are treated as Gaussian distributions and statistical fluctuations are simulated using Poisson statistics. If the calculated confidence level CL = 1-Cl_s does not reach the requested value (95%) the expected signal is scaled by a factor x_f and the the limit calculation is repeated. Assuming the predicted signal is $N_s = \sigma_s L \epsilon_s$ where σ_s is the signal cross-section, L is luminosity and ϵ_s is the signal efficiency then the 95% CL limit can be taken as $x_f \sigma_s$ [59].

Figure 8 shows the behaviour of the observed Cl_s for different tested values of the instanton cross-section, computed with 2M toy MC simulations per point. Also the expected median upper-limit (i.e. the background-only hypothesis) with the bands corresponding to $\pm 1\sigma$ and $\pm 2\sigma$ fluctuations is shown. The observed limit is 1.6 pb at 95% CL in comparison with the theoretically predicted cross-section of 10 pb.

8 Conclusion

A search for QCD instanton-induced processes is presented in deep-inelastic scattering at the electron-proton collider HERA in the kinematic region defined by the Bjorken-scaling variable $x > 10^{-3}$, the inelasticity $0.2 < y < 0.7$ and the photon virtuality $150 < Q^2 < 15000$ GeV^2. The search is performed using H1 data corresponding to an integrated luminosity of 357 pb^{-1}.

Several observables of the hadronic final state of the events are exploited to identify a potentially instanton-enriched domain. Two Monte Carlo models, RAPGAP and DJANGOH, are used to estimate the background from the standard DIS processes, and the instanton-induced scattering processes are modeled by the program QCDINS. In order to extract the expected signal a multivariate data analysis technique is used. No evidence for QCD instanton-induced processes is observed Using CL_s statistical method the upper limit on the instanton cross-section of 1.6 pb at 95% CL is set. This result suggests the exclusion of the theoretically predicted cross-section of 10 pb.

Acknowledgements

We thank A. Ringwald and F. Schrempp for many helpfull discussions. We are grateful to the HERA machine group whose outstanding efforts have made this experiment possible. We thank the engineers and technicians for their work in constructing and maintaining the H1 detector, our funding agencies for financial support, the DESY technical staff for continual assistance and the DESY directorate for support and for the hospitality which they extend to the non DESY members of the collaboration.

References

[1] G. 't Hooft, *Symmetry Breaking Through Bell-Jackiw Anomalies*, Phys. Rev. Lett. **37** (1976) 8; G. 't Hooft, *Computation Of The Quantum Effects Due To A Four-Dimensional Pseudoparticle*, Phys. Rev. D **14** (1976) 3432; [Erratum-ibid. D **18** (1976) 2199].

[2] A. A. Belavin, A. M. Polyakov, A. S. Shvarts and Y. S. Tyupkin, *Pseudoparticle Solutions Of The Yang-Mills Equations*, Phys. Lett. B **59** (1975) 85.

[3] A. Ringwald and F. Schrempp, in: *Quarks '94* (Vladimir, Russia, 1994), D. Grigoriev et al., Eds., Proc. of the 8th Int. Seminar, pp. 170, hep-ph/9411217.

[4] S. Moch, A. Ringwald and F. Schrempp, *Instantons in deep-inelastic scattering: The simplest process*, Nucl. Phys. B **507** (1997) 134 [hep-ph/9609445].

[5] A. Ringwald and F. Schrempp, *Instanton-induced cross-sections in deep-inelastic scattering*, Phys. Lett. B **438** (1998) 217 [hep-ph/9806528].

[6] A. Ringwald and F. Schrempp, *Confronting instanton perturbation theory with QCD lattice results*, Phys. Lett. B **459** (1999) 249 [hep-lat/9903039].

[7] M. Gibbs et al., in: *Future Physics at HERA* (Hamburg, Germany, 1996), G. Ingelman, A. deRoeck, and R. Klanner, Eds., vol. 1, p. 509.

[8] T. Carli, J. Gerigk, A. Ringwald and F. Schrempp, *QCD instanton-induced processes in deep-inelastic scattering: Search strateg, in: Monte Carlo Generators for HERA Physics* (Hamburg, Germany, 1999), A. Doyle, G. Ingelman, H. Jung and G. Grindhammer, Eds, p.329, hep-ph/9906441.

[9] A. Ringwald and F. Schrempp, *Zooming-in on instantons at HERA*, Phys. Lett. B **503** (2001) 331 [hep-ph/0012241].

[10] A. Ringwald and F. Schrempp, *QCDINS 2.0: A Monte Carlo generator for instanton-induced processes in deep-*, Comput. Phys. Commun. **132** (2000) 267 [hep-ph/9911516].

[11] A. Ringwald and F. Schrempp, in: *New Trends in HERA Physics* (Schloss Ringberg, Tegernsee, Germany, 1999), G. Grindhammer, B. Kniehl, G. Kramer and W. Ochs, Eds., pp. 203, hep-ph/9909338.

[12] F. Schrempp,*Tracking QCD-instantons*, J. Phys. G **28** (2002) 915 [hep-ph/0109032].

[13] C. Adloff *et al.* [H1 Collaboration], *Search for QCD instanton-induced processes in deep-inelastic scattering at HERA*, Eur. Phys. J. C **25** (2002) 495 [arXiv:hep-ex/0205078].

[14] S. Chekanov *et al.* [ZEUS Collaboration], "Search for QCD instanton induced events in deep inelastic ep scattering at HERA," Eur. Phys. J. C **34** (2004) 255 [hep-ex/0312048].

[15] M. Gibbs, A. Ringwald and F. Schrempp, in: *Proc. DIS 1995* (Paris, France, 1995), J.-F. Laporte and Y. Sirois, Eds., pp. 341, hep-ph/9506392.

[16] G. Marchesini et al., *HERWIG: A Monte Carlo event generator for simulating hadron emission reaction*, Comput. Phys. Commun. **67** (1992) 465.

[17] J. Gerigk, *Dipl. Thesis University of Hamburg (unpublished) and MPI-PhE/98-20* (Nov. 1998), also at http://www-h1.desy.de/publications/theses_list.html

[18] B. Koblitz [H1 Collaboration], *A search for instantons at HERA*, J. Phys. G **28** (2002) 927 [hep-ex/0110042].

[19] B. Koblitz, *Ph.D. thesis University of Hamburg 2002, MPI-PhE/2002-07*, also at http://www-h1.desy.de/publications/theses_list.html.

[20] K. Nakamura *et al.* [Particle Data Group Collaboration], *Review of particle physics*, J. Phys. G G **37** (2010) 075021.

[21] I. Abt *et al.* [H1 Collaboration], *The H1 detector at HERA*, Nucl. Instrum. Meth. **A386** (1997) 310.

[22] I. Abt *et al.* [H1 Collaboration], *The Tracking, calorimeter and muon detectors of the (H1 Collaboration) experiment at HERA*, Nucl. Instrum. Meth. **A386** (1997) 348.

[23] B. Andrieu *et al.* [H1 Calorimeter Group], *The H1 liquid argon calorimeter system*, Nucl. Instrum. Meth. **A336** (1993) 460.

[24] R. D. Appuhn *et al.* [H1 SpaCal Group], *The H1 lead/scintillating fiber calorimeter*, Nucl. Instrum. Meth. **A386** (1997) 397.

[25] B. Andrieu *et al.* [H1 Calorimeter Group], *Results from pion calibration runs for the H1 liquid argon calorimeter and comparisons with simulations*, Nucl. Instrum. Meth. **A336** (1993) 499.

[26] B. Andrieu *et al.* [H1 Calorimeter Group], *Beam tests and calibration of the H1 liquid argon calorimeter with electrons*, Nucl. Instrum. Meth. **A350** (1994) 57.

[27] J. Becker *et al.*, *A Vertex trigger based on cylindrical multiwire proportional chambers*, Nucl. Instrum. Meth. **A586** (2008) 190 [physics/0701002].

[28] P. J. Laycock *et al.*, *The H1 forward track detector at HERA II*, submitted to JINST, [arXiv:1206.4068].

[29] D. Pitzl *et al.*, *The H1 silicon vertex detector*, Nucl. Instrum. Meth. **A454** (2000) 334 [hep-ex/0002044].

[30] B. List, *The H1 central silicon tracker*, Nucl. Instrum. Meth. **A501** (2001) 49.

[31] I. Glushkov, *D* meson production in deep inelastic electron-proton scattering with the forward and backward silicon trackers of the H1 experiment at HERA*, PhD thesis, Humboldt University, Berlin, 2007, (available at http://www-h1.desy.de/publications/theses_list.html).

[32] J. Kretzschmar, *A precision measurement of the proton structure function F2 with the H1 experiment*, PhD thesis, Humboldt University, Berlin, 2008, (available at http://www-h1.desy.de/publications/theses_list.html).

[33] T. Nicholls *et al.* [H1 SPACAL Group Collaboration], *Performance of an electromagnetic lead / scintillating fiber calorimeter for the H1 detector*, Nucl. Instrum. Meth. A **374** (1996) 149.

[34] F. D. Aaron *et al.* [H1 Collaboration], *Determination of the Integrated Luminosity at HERA using Elastic QED Compton Events*, Eur. Phys. J. C **72** (2012) 2163 [arXiv:1205.2448 [hep-ex]].

[35] V. Andreev *et al.* [H1 Collaboration], *Measurement of Multi Jet Production in ep Collisions at High Q^2 and Determination of the Strong Coupling Constant $\alpha_s(m_Z)$* , in preparation.

[36] H. Jung, *Hard diffractive scattering in high-energy e p collisions and the Monte Carlo*, Comput. Phys. Commun. **86** (1995) 147;
see updates on http://www.desy.de/$\sim$jung.

[37] M. Bengtsson and T. Sjöstrand, *Parton Showers In Leptoproduction Events*, Z. Phys. C **37** (1988) 465.

[38] V. N. Gribov and L. N. Lipatov, *Deep Inelastic E P Scattering In Perturbation Theory*, Yad. Fiz. **15** (1972) 781 [Sov. J. Nucl. Phys. **15** (1972) 438]; Y. L. Dokshitzer, *Calculation Of The Structure Functions For Deep Inelastic Scattering And E+ E*, (In Russian), Sov. Phys. JETP **46** (1977) 641 [Zh. Eksp. Teor. Fiz. **73** (1977) 1216]; G. Altarelli and G. Parisi, *Asymptotic Freedom In Parton Language*, Nucl. Phys. B **126** (1977) 298.

[39] K. Charchula, G. A. Schuler and H. Spiesberger, *Combined QED and QCD radiative effects in deep inelastic lepton - proton scattering: The Monte Carlo generator DJANGO6*, Comput. Phys. Commun. **81** (1994) 381.

[40] G. Gustafson and U. Pettersson, *Dipole Formulation Of QCD Cascades*,Nucl. Phys. B **306** (1988) 746;

[41] L. Lönnblad, *ARIADNE version 4: A Program for simulation of QCD cascades implementing the*, Comput. Phys. Commun. **71** (1992) 15.

[42] B. Andersson, G. Gustafson, G. Ingelman and T. Sjöstrand, *Parton Fragmentation And String Dynamics*,Phys. Rept. **97** (1983) 31.

[43] T. Sjöstrand and M. Bengtsson, *The Lund Monte Carlo For Jet Fragmentation And E+ E- Physics: Jetset Version*, Comput. Phys. Commun. **43** (1987) 367.

[44] J. Pumplin, D. R. Stump, J. Huston, H. L. Lai, P. M. Nadolsky and W. K. Tung, *New generation of parton distributions with uncertainties from global QCD analysis*, JHEP **0207** (2002) 012 [hep-ph/0201195].

[45] H. L. Lai *et al.* [CTEQ Collaboration], *Global QCD analysis of parton structure of the nucleon: CTEQ5 parton distributions*, Eur. Phys. J. C **12** (2000) 375 [hep-ph/9903282].

[46] M. Peez, *Recherche de déviations au Modèl Standard dans les processus de grande énergie transverse sur le collisionneur électron - proton*, PhD thesis, Univ. Lyon, 2003, DESY-THESIS-2003-023, (available at http://www-h1.desy.de/publications/theses_list.html).

[47] B. Portheault, *Première mesure des sections efficaces de courant chargé et neutre avec le faisceau de positrons polarisé à HERA II et analyses QCD-électrofaible*, PhD thesis, Univ. Paris XI Orsay, LAL-05-05,2005,(available at http://www-h1.desy.de/publications/theses_list.html).

[48] C. Adloff *et al.* [H1 Collaboration], *Measurement and QCD analysis of neutral and charged current cross sections at HERA*, Eur. Phys. J. **C30** (2003) 1 [hep-ex/0304003].

[49] U. Bassler and G. Bernardi, *Structure function measurements and kinematic reconstruction at HERA*, Nucl. Instrum. Meth. A **426** (1999) 583 [hep-ex/9801017].

[50] S. D. Ellis and D. E. Soper, *Successive combination jet algorithm for hadron collisions*, Phys. Rev. D **48** (1993) 3160 [hep-ph/9305266].

[51] M. Cacciari and G. P. Salam, *Dispelling the N^3 myth for the k_t jet-finder*, Phys. Lett. B **641** (2006) 57 [hep-ph/0512210].

[52] T. Sjostrand, “High-energy physics event generation with PYTHIA 5.7 and JETSET 7.4,” Comput. Phys. Commun. **82** (1994) 74,[arXiv:hep-ph/9508391].

[53] G. C. Fox and S. Wolfram, “Event Shapes in e+ e- Annihilation,” Nucl. Phys. B **149** (1979) 413 [Erratum-ibid. B **157** (1979) 543].

[54] R. Kogler, *Measurement of jet production in deep-inelastic ep scattering at HERA*, PhD thesis, Univ. Hamburg, DESY-THESIS-2011-003, MPP-2010-175,2010.

[55] A. Hocker, J. Stelzer, F. Tegenfeldt, H. Voss, K. Voss, A. Christov, S. Henrot-Versille and M. Jachowski *et al.*, *TMVA - Toolkit for Multivariate Data Analysis*, PoS ACAT (2007) 040 [physics/0703039 [PHYSICS]].

[56] A. L. Read, “Modified frequentist analysis of search results (The CL(s) method),” 1st Workshop on Confidence Limits,CERN,Geneva, Switzerland,17-18 Jan 2000, 81-101, CERN-OPEN-2000-205.

[57] T. Junk, “Confidence level computation for combining searches with small statistics,” Nucl. Instrum. Meth. A **434** (1999) 435 [hep-ex/9902006].

[58] P. Bock, “Computation of confidence levels for exclusion or discovery of a signal with the method of fractional event counting,” JHEP **0701** (2007) 080 [hep-ex/0405072].

[59] Wade Fisher, “Calculating Limits for Combined Analysis,” D∅ Note # 4975(January 23, 2006.

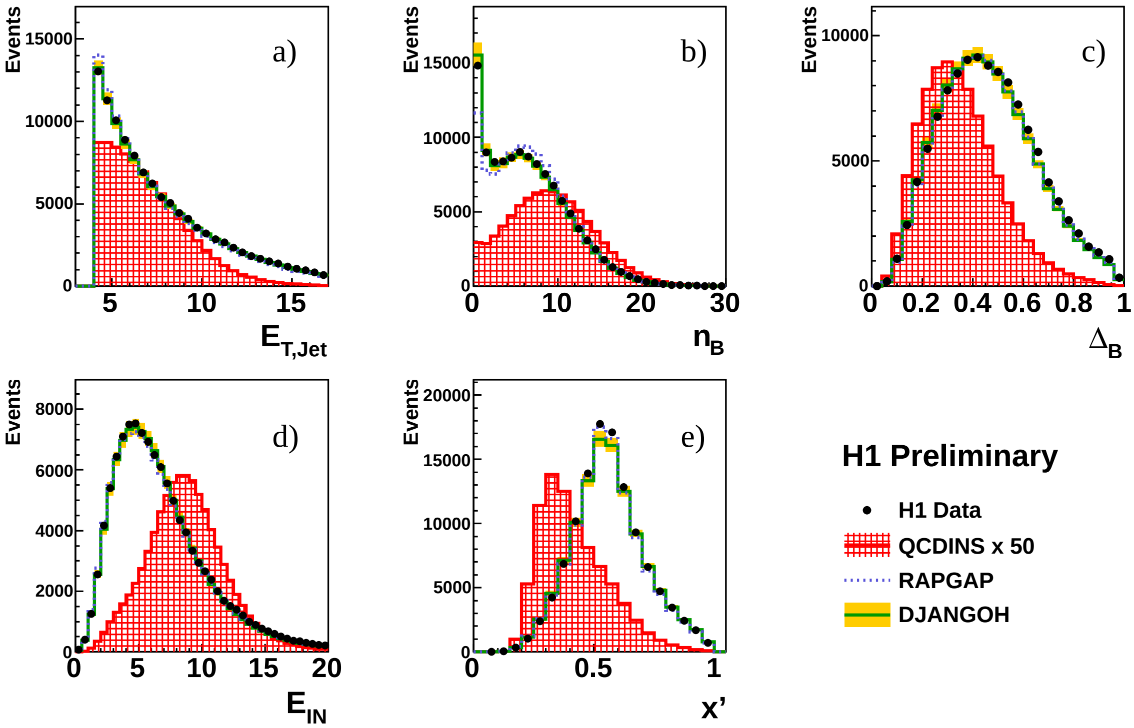

Figure 2: Distributions of the observables used in the multivariate analysis : (a) the transverse current jet energy, $E_{T,Jet}$, (b) the charged particle multiplicity in the I-band, n_B, two variables measuring the azimuthal isotropy of the event (c) Δ_B and (d) E_{IN}, and (e) the reconstructed instanton kinematic variable x'. Data (filled circles), the QCD model background Monte Carlo simulations (dotted and solid lines) and the QCDINS prediction scaled up by a factor of 50 (hatched) are shown. The error band, shown only for DJANGOH MC, represents the statistical and systematic uncertainties added in quadrature.

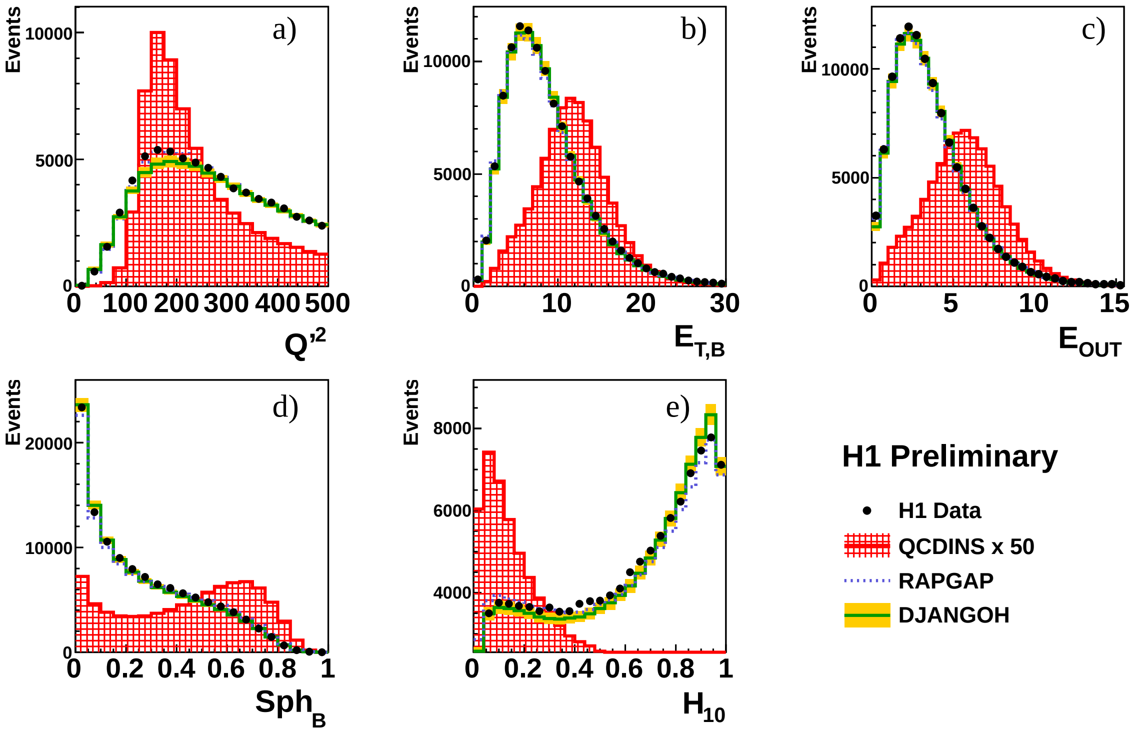

Figure 3: Distributions of the observables unused in the multivariate analysis: the reconstructed instanton kinematic variable, Q'^2 , the total scalar transverse energy of all hadronic final state objects in the I-band,$E_{T,B}$, two variables measuring the azimuthal isotropy of the event E_{OUT} and Sph_B, and the Fox-Wolfram moment H_{10}. Data (filled circles), the QCD model background Monte Carlo simulations (dotted and solid lines) and the QCDINS prediction scaled up by a factor of 50 (hatched) are shown. The error band, shown only for DJANGOH MC, represents the statistical and systematic uncertainties added in quadrature.

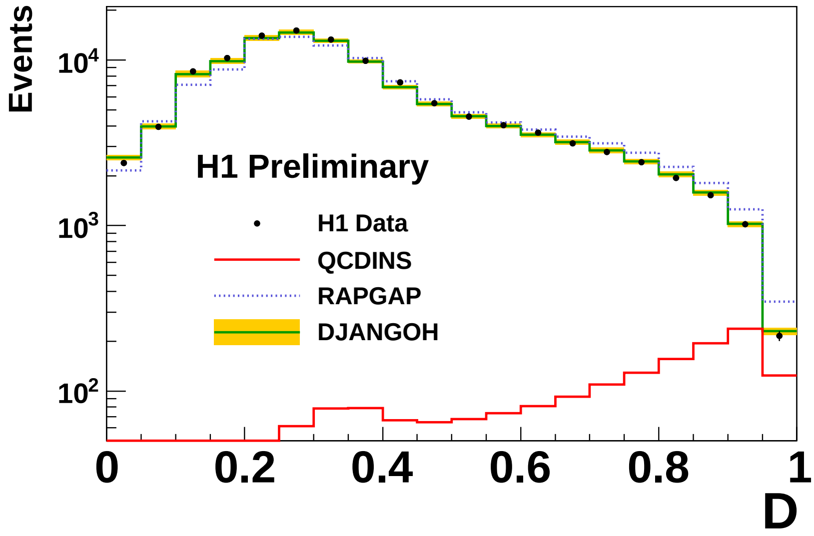

Figure 4: The distribution of the discriminator from the PDERS method. Data (filled circles), the QCD model background Monte Carlo simulations (dotted and solid lines) and the QCDINS prediction (hatched) are shown. The error band, shown only for DJANGOH MC, represents the statistical and systematic uncertainties added in quadrature.

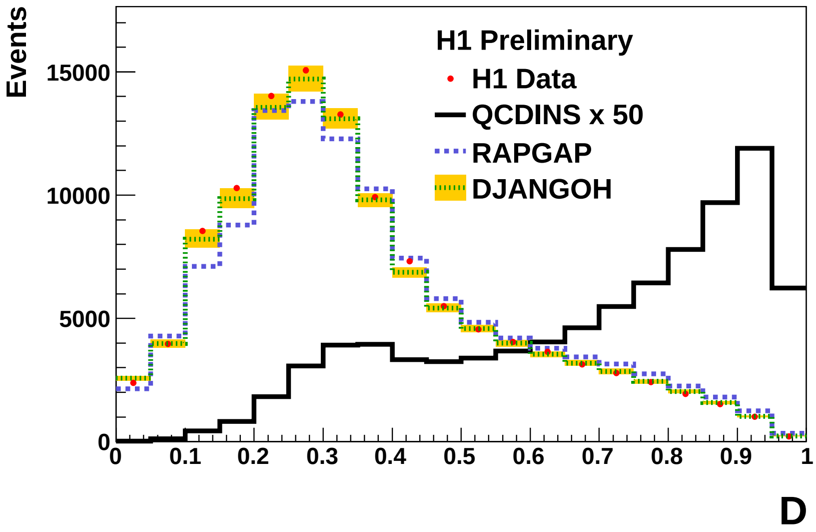

Figure 5: The distribution of the discriminator from the PDERS method. The error band represents the statistical and systematic uncertainties added in quadrature.

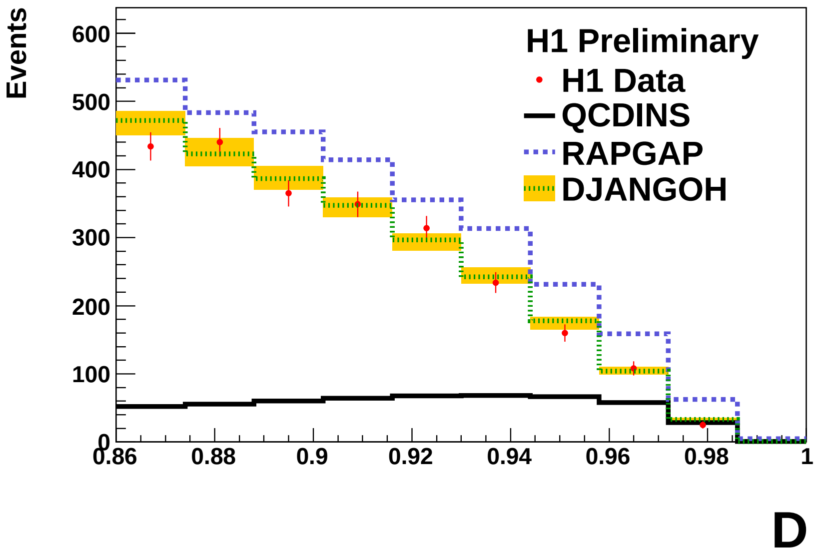

Figure 6: The distribution of the discriminator from the PDERS method in the signal region ($D > 0.86$). The error bands represent the statistical and systematic uncertainties added in quadrature.

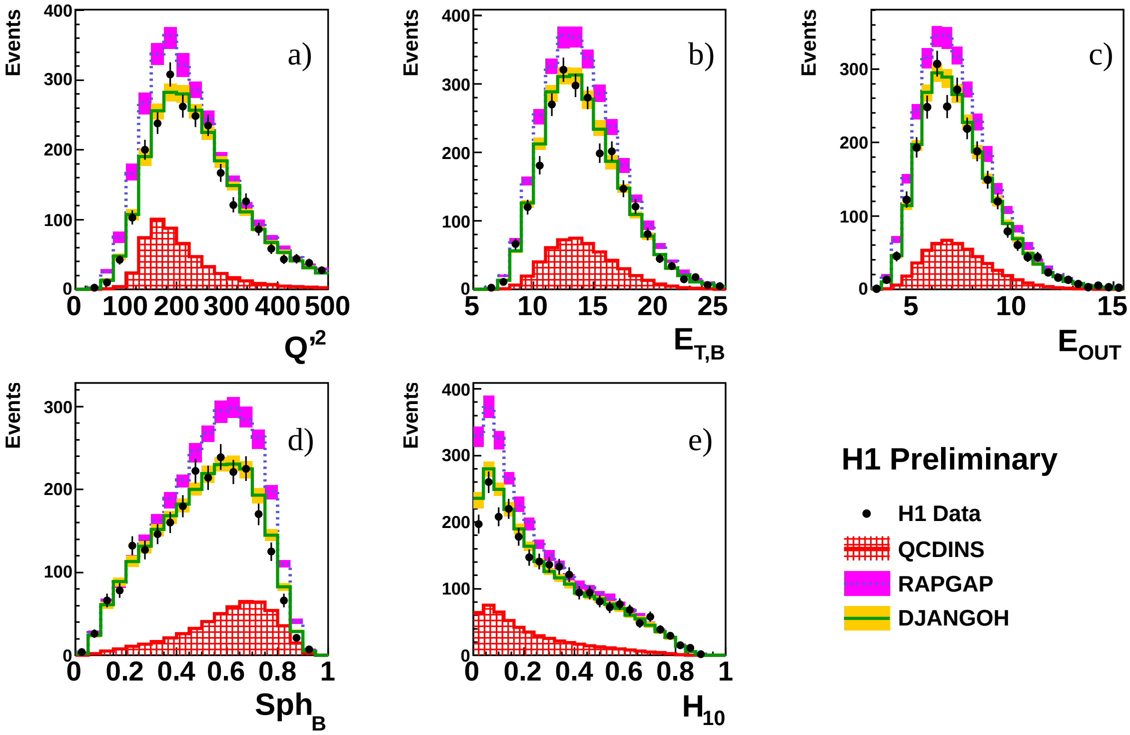

Figure 7: Distributions of the observables unused in the multivariate analysis after the cut on the discriminator ($D > 0.86$) to enrich the expected signal: (a) the reconstructed instanton kinematic variable, Q'^2 , (b) the total scalar transverse energy of all hadronic final state objects in the I-band,$E_{T,B}$, two variables measuring the azimuthal isotropy of the event (c) E_{OUT} and (d) the sphericity Sph_B, and the Fox-Wolfram moment H_{10}. Data (filled circles), the QCD model background Monte Carlo simulations (dotted and solid lines) and the QCDINS prediction (hatched) are shown. The error bands represent the statistical and systematic uncertainties added in quadrature.

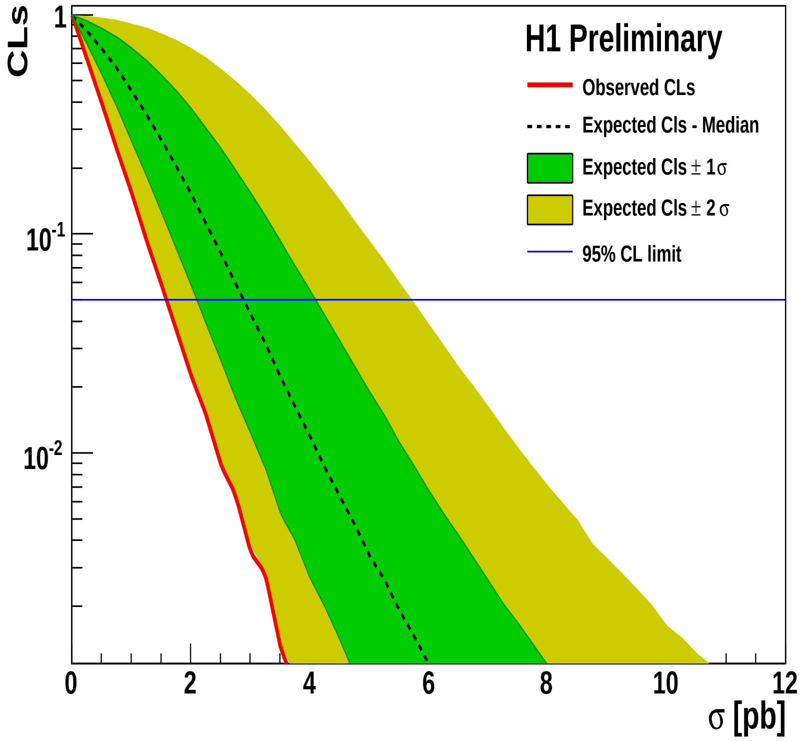

Figure 8: Observed CL_s (solid, red line) as a function of the instanton cross section. The 95% CL limit is indicated by the horizontal (blue) line. The dark and light bands correspond to $\pm 1\sigma$ and $\pm 2\sigma$ fluctuations on the expectation (dashed line).